PERGAMON

Journal of Structural Geology 23 (2001) 1917–1932

JOURNAL OF STRUCTURAL GEOLOGY

www.elsevier.com/locate/jstrugeo

Mechanisms and orientation of melt segregation paths during pure shearing of a partially molten rock analog (norcamphor–benzamide)

Claudio L. Rosenberg*, Mark R. Handy

Fachbereich Geowissenschaften, Fachrichtung Geologie, Malteser Strasse 74-100 12249 Berlin, Germany

Received 6 December 1999; revised 23 January 2001; accepted 7 February 2001

Abstract

In-situ deformation experiments were performed on partially molten analog materials (norcamphor in the presence of a benzamide–norcamphor melt) undergoing pure shearing at a constant melt fraction of 0.13. Melt in the samples induces a strain-dependent transition from purely dislocation creep to dislocation creep associated with minor intergranular fracturing and grain boundary sliding (GBS). Intergranular fractures drain the melt from initially isotropic melt pockets to grain boundaries. Along such boundaries, grain-boundary migration recrystallization is inhibited, while GBS occurs. Intergranular melt pockets occur along grain boundaries oriented subparallel to the shortening direction, but melt must have migrated parallel to the elongation direction of the samples, as indicated by melt accumulations at both extruding ends of the sample. Intergranular melt pockets parallel to the elongation direction were only rarely observed, because melt was rapidly expelled from these sites. Nevertheless, these grain boundaries are the pathways of melt segregation in the samples.

Keywords: Melt; Segregation; Partially molten rocks; In-situ deformation; Synmagmatic deformation; Microstructures; Deformation mechanisms

1. Introduction

Geochemical (Bodinier, 1988) as well as structural and microstructural (e.g. McLellan, 1988; Berger and Kalt, 1999) studies have shown that deformation enhances melt segregation from partially molten rocks. This process is characterized by the development of stromatic migmatites under dynamic conditions, in contrast to patchy migmatites in which the melt is homogeneously distributed in the protolith under static conditions (McLellan, 1988; Berger and Kalt, 1999). In order to understand the mechanisms by which partial melts that formed at phase boundaries (Mehnert et al., 1973) collect into larger pockets or dykes, and thereby escape from their source region, we need to reconstruct the grain-scale pathways of these melts.

These pathways are generally obliterated in naturally deformed rocks, because intergranular melt films crystallize in optical continuity with the adjacent grains during slow crystallization. Experimental studies may provide important insights into these processes. In experimental coaxial deformation of granitic and mantle rocks in the presence of low melt fractions (<0.15) at high confining pressure, the magnitude of the differential stress is the main factor controlling melt distribution (Daines, 1997; Daines and Kohlstedt, 1997; Gleason et al., 1999) if deformation occurs by a viscous-type of flow (dislocation or diffusion creep). Under such conditions, melt pockets are oriented at low angles to the principal stress direction, which is therefore inferred to be the main direction of melt migration on the grain- and map-scales (e.g. Daines and Kohlstedt, 1997). Syntectonic melt pockets oriented at a high angle to the foliation plane have been described in natural rocks (see Nicolas and Jackson (1982) for mantle rocks and Rosenberg and Riller (2000) for granitic rocks). More often, however, syntectonic melt segregations in crustal rocks (quartzo–feldspathic leucosomes) and mantle rocks (plagioclase and clinopyroxene) are oriented parallel or subparallel to the foliation plane (e.g. Weber and Barbey (1986) and Jousselin and Mainprice (1999) for crustal and mantle rocks, respectively). This orientation suggests a high angle ($\geqq 45°$) between the orientation of melt pockets and the principal compressive stress direction, if one assumes that the foliation plane corresponds to the shear plane. This, in turn, indicates that the mechanisms by which melt migrates in experiments may be different than those that operate in nature.

Regardless of the orientation of melt pockets with respect to the foliation plane and/or principal stress directions, the

* Corresponding author. Tel.: +49-30-8387-0902; fax: +49-30-775-9078.

E-mail address: cla@zedat.fu-berlin.de (C.L. Rosenberg).

0191-8141/01/$ - see front matter
PII: S0191-8141(01)00037-2

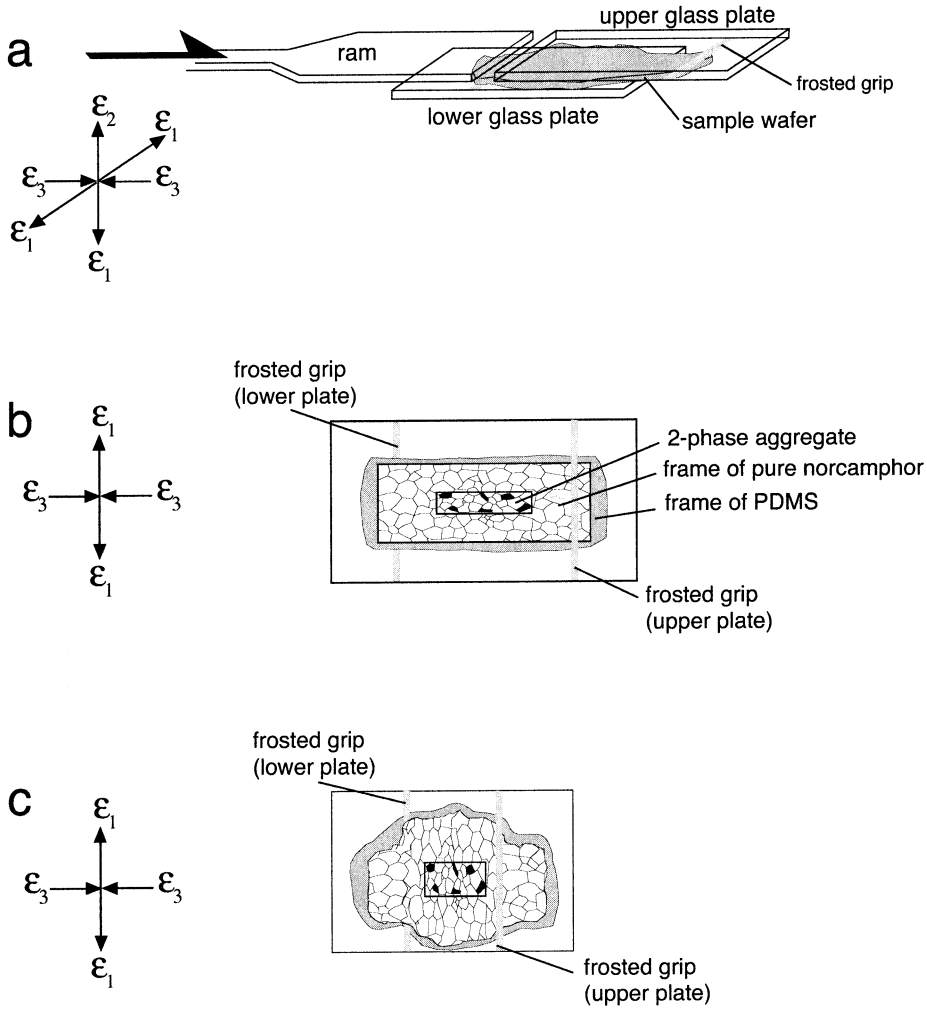

Fig. 1. Experimental configuration. $\varepsilon 1$, $\varepsilon 2$, $\varepsilon 3$ denote finite strain axes. (a) View of glass slides containing sample and confining media. (b) Sample configuration before pure shearing. The norcamphor–benzamide aggregate is located between the frosted grips and enclosed in a frame of norcamphor. This in turn is sealed within a frame of PDMS. (c) Sample configuration after pure shearing. Note the 'barreling' of the sample perpendicular to the principal shortening direction.

process of melt migration through a deforming aggregate is still a subject of debate. We address a number of questions in this work. (1) What mechanisms allow melt pockets or films to migrate along the grain boundaries? Although it has been shown in experiments that melt migrates along grain boundaries (e.g. Dell'Angelo and Tullis, 1988) it remains unclear whether melt migration is driven by intergranular fracturing (Rosenberg and Riller, 2000), possibly involving subcritical crack growth (e.g. Rubin, 1997), dissolution at grain boundaries (Jin et al., 1994), mean stress gradients (Daines and Kohlstedt, 1997) or some combination of these phenomena; (2) How is the orientation of intergranular melt pockets related to melt flow on larger scales? The orientation of intergranular melt pockets is commonly considered to coincide with the dominant flow direction of melt through the rock. However, Dell'Angelo and Tullis (1988) showed that significant melt flow occurred along grain boundaries oriented subperpendicular to the principal shortening direction even though melt pockets within the deformed sample were oriented subparallel to the principal shortening direction; (3) Is there a minimum melt fraction, corresponding to a percolation threshold (e.g. Maaløe, 1985; Sawyer, 1994; Vigneresse et al., 1996) below which segregation is not possible?

In order to investigate the relationship between melt migration and grain-scale deformation, we performed a series of pure shear, 'see-through' deformation experiments using partially molten analog materials. This allowed us to record the change in geometry and spatial distribution of melt pockets and grain-boundaries during deformation. In a previous experiment (Rosenberg and Handy, 2000), we deformed a partially molten benzamide–norcamphor aggregate in simple shear in order to investigate the relationship between strain localization and melt segregation during synkinematic melting. We showed that melt-bearing shear bands form after small strain increments, and that these

dilatant shear bands interconnect at higher shear strains. The interconnected shear bands form pathways for the segregation of melt at low angles to the shear zone boundary. The pure shear experiments reported here contrasted with our previous work in two important respects. First, the geometry of intergranular melt was perpendicular to the melt segregation direction, i.e. from the central part of the sample to the sinks at the lengthening ends of the sample. Second, melting occurred before, rather than during deformation, and is not affected by any geometrical changes due to increasing melt volume.

2. Experimental materials and conditions

The experiments involved shearing a thin wafer of organic material between two glass plates (thin section plates) in a modified Means–Urai deformation rig (see Means (1989) and Bauer et al. (2000) for detailed descriptions). The experimental configuration is illustrated schematically in Fig. 1. The sample preparation technique used in this study is similar to that used in Rosenberg and Handy (2000), and is described briefly again below.

We conducted experiments under plane strain, pure shear conditions at an axial strain rate of $1.7 \times 10^{-4}\ s^{-1}$. Experiments were carried out with samples consisting of 97 wt% norcamphor ($C_7H_{10}O$, probably hexagonal: Bons, 1993) mixed with 3 wt% benzamide ($C_6H_5CONH_2$, monoclinic). A eutectic melt formed at 42°C, significantly below the melting temperatures of pure norcamphor (96–98°C) and benzamide (132°C). The eutectic composition contains approximately 20 wt% benzamide and 80 wt % norcamphor. Small amounts of fine-grained (average grain size: 9 μm) corundum grinding powder were mixed with the norcamphor and benzamide during preparation to provide strain markers during the deformation experiments (e.g. Means, 1983). These particles did not hinder grain-boundary mobility. The aggregate was cold pressed at room temperature to a thickness of 130–180 μm. An 8 mm × 4 mm tablet was cut from the pressed aggregate and positioned between the frosted grips on the thin sections (Fig. 1b) in such a way that it did not come into contact with the frosted grips themselves. The tablet of norcamphor–benzamide was then enclosed within a frame of pure norcamphor (Fig. 1b). This frame of norcamphor melted at a higher temperature than the mixture and therefore formed a barrier for the melt generated within the enclosed norcamphor–benzamide aggregate. To further ensure that the melt did not escape from the experimental system during deformation, the norcamphor–benzamide aggregate and the norcamphor frame were both enclosed in a frame of polydimethyl–siloxane or PDMS (Fig. 1; see Weijermars (1986) for a description of its rheology).

The samples were annealed within the deformation apparatus at 38°C for 4–7 days. The mean apparent diameter of the annealed norcamphor and benzamide grains in the undeformed aggregate was, respectively, 200–400 μm and 50 μm. For comparison, dry experiments were performed at 38°C and experiments in the presence of melt at 45°C.

The microstructural evolution during deformation was recorded with color slides and digital movies taken from a macroscope (a microscope with long focal operating distance) at a maximum magnification of 64×. Identifying the melt during the experiments was difficult because the melt is opaque in crossed polarized light and therefore indistinguishable from crystals and crystal domains at complete optical extinction. We overcame this problem by using reflected light microscopy in addition to polarized light to distinguish the melt from the solids. In some cases, we also periodically chilled the sample, quenching the melt to a brown, microcrystalline aggregate that could be easily distinguished from the solid norcamphor and benzamide grains. The melt volume proportion in the samples was calculated from the areal proportion of quenched melt in the samples, as determined with the program NIH-Image (Rasband, 1997).

3. Melting, crystallization and recrystallization under stress-annealing

To examine the role of deformation on melt topology, a series of melting experiments was performed without deformation and compared with deformation experiments. Samples were enclosed in the apparatus and, were submitted to an anisotropic stress field (see Herwegh and Handy (1996) for discussion). Although the resulting microstructure corresponds to that observed during static growth experiments, the samples actually underwent stress-annealing.

Melt topology during static crystallization is controlled by the interfacial energy ratios between solid–solid and solid–melt (e.g. Laporte et al., 1997). Although statistical measurements of melt–norcamphor wetting angles are still lacking, we examined norcamphor grain contacts during static crystallization in order to compare melt distributions under static and dynamic conditions. These observations show that melt–norcamphor–norcamphor dihedral angles are less than 60°, indicating that melt is distributed along a network of interconnected channels rather than in isolated pockets (e.g. Laporte et al., 1997). The large number of grain boundaries wetted by a melt film confirm this inference. These high angle boundaries suggest that the surface–energy ratio of norcamphor–norcamphor to melt–norcamphor is similar to that measured for most silicate minerals in contact with a granitic melt (review in Laporte et al. (1997)).

In contrast to the static crystallization experiments, the stress-annealing experiments yielded a melt distribution that was controlled by the distribution of norcamphor–benzamide phase boundaries. Melt formed primarily along such boundaries. This observation is well known from experiments on

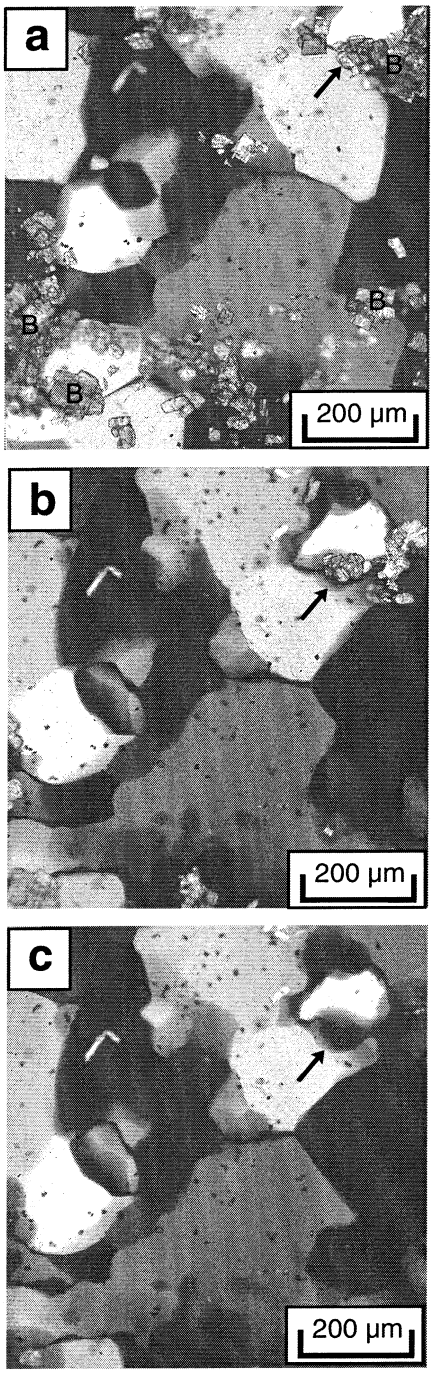

Fig. 2. Melting of a benzamide–norcamphor mixture under stress-annealing conditions. Benzamide grains are the small, light rectangular plates (B). Norcamphor grains are grains containing the corundum strain markers (black dots). (a) Microstructure previous to melting, after 5 days stress-annealing at 38.5°C. (b) Microstructure during melting, at $T = 43$°C, 1 h after the onset of melting. The dark gray and black areas indicated by the arrows are melt pockets that replace the benzamide grains and part of the surrounding norcamphor. (c) Microstructure during melting, at $T = 44$°C, 3 h after the onset of melting. Note the lobate shape of many grain boundaries.

silicate systems (Mehnert et al., 1973). We induced melting by increasing the temperature above the solidus (42°C) of the norcamphor–benzamide aggregate. Melting initiated along the grain boundaries of neighboring norcamphor and benzamide grains, as expected for a eutectic melt (e.g. Mehnert et al., 1973) and proceeded until the benzamide grains had entirely melted. We inferred the presence of melt from the appearance of black haloes (observed with crossed polarizers) around the benzamide grains (Fig. 2) and from the gradual disappearance of benzamide grains (Fig. 2).

Rapid grain-boundary migration and grain growth of norcamphor occurred as soon as melt appeared in the sample. Fig. 3 shows different stages of grain growth in one part of the sample as the temperature was increased from 51 to 65°C. Grain boundaries migrated at a rate of approximately 0.1 μm s^{-1}, and the average grain size nearly doubled within 10 h (Fig. 2b and c). Both grain growth and grain-boundary mobility can be entirely ascribed to the presence of melt, because this same temperature increase (14°C) in melt-free norcamphor samples does not result in any changes of grain size or grain boundary mobility rate. Rapid grain-boundary migration initially resulted in very lobate grain boundaries (Figs. 2 and 3), similar to those observed during high-temperature dynamic recrystallization. Only later did grain boundaries straighten, presumably to minimize surface energy.

The driving force of this melt-induced grain-boundary migration is not clear, but Daines (1997, quoted in Bai et al., 1997) also observed anomalously high grain growth rates in the presence of melt. The surface area of grain boundaries increased upon melting due to the formation of convex melt pockets along grain boundaries (Fig. 2). Moreover, the equilibrium geometry of norcamphor–benzamide boundaries was transformed into a melt–norcamphor boundary, which probably has a different surface energy than the solid norcamphor–benzamide boundaries. As a consequence, that boundary acquired a new geometry.

4. Melt-free deformation experiments

The presence of melt may activate deformation mechanisms not normally operative in melt-free samples at the same pressure and temperature (Dell'Angelo and Tullis, 1988). In order to assess the effect of melt on the deformation mechanisms operative in our samples, melt-free deformation experiments were performed and compared with experiments in the presence of melt.

The melt-present experiments were performed with samples consisting of norcamphor grains and a melt of benzamide–norcamphor composition. No solid benzamide grains were present during deformation. In order to constrain the effect of melt on the microstructure of the solid grains, melt-free experiments with monomineralic norcamphor aggregates were conducted at 45°C,

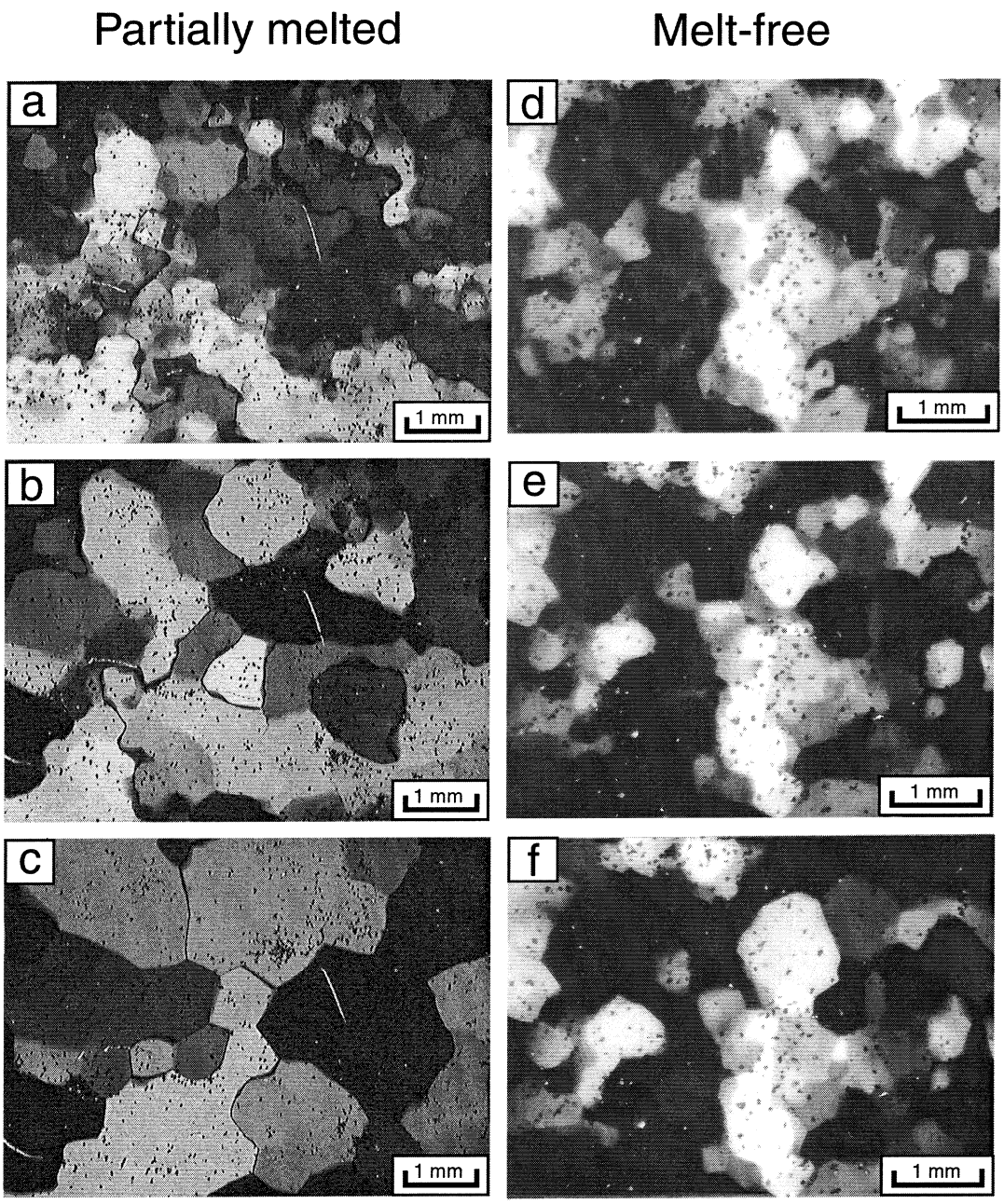

Fig. 3. Grain-growth at stress-annealing conditions, in the presence (a–c) and in the absence (d–f) of melt. (a) Norcamphor aggregate containing a norcamphor–benzamide melt at 51°C. (b) Same area of the sample as (a), photographed after 2 h and 10 min at 65°C. (c) Same area of the sample as (a) and (b), photographed after 10 h at 65°C. Black dots are corundum particles used as strain markers. (d) Norcamphor aggregate after 4 days of stress-annealing at 51°C. (e) Same area of the sample as (a), photographed after 2 h and 10 min at 65°C. (f) Same area of the sample as (a) and (b), photographed after 10 h at 65°C.

corresponding to a homologous temperature of 0.86. This is the same temperature as used for the experiments in the presence of melt. A shape preferred orientation (SPO) defined by the alignment of the long axes of norcamphor grains developed after a shortening of 5–10%. Norcamphor grains contained subgrains and deformation bands and underwent dynamic recrystallization by grain-boundary migration (Fig. 4a), suggesting deformation by dislocation creep. This interpretation is also supported by the development of a crystallographic preferred orientation, indicated by the fact that most grains showed the same interference color (Fig. 4a).

5. Deformation experiments in the presence of melt

5.1. Initial configuration

Prior to deformation, samples were melted under static conditions until the benzamide grains completely dis-

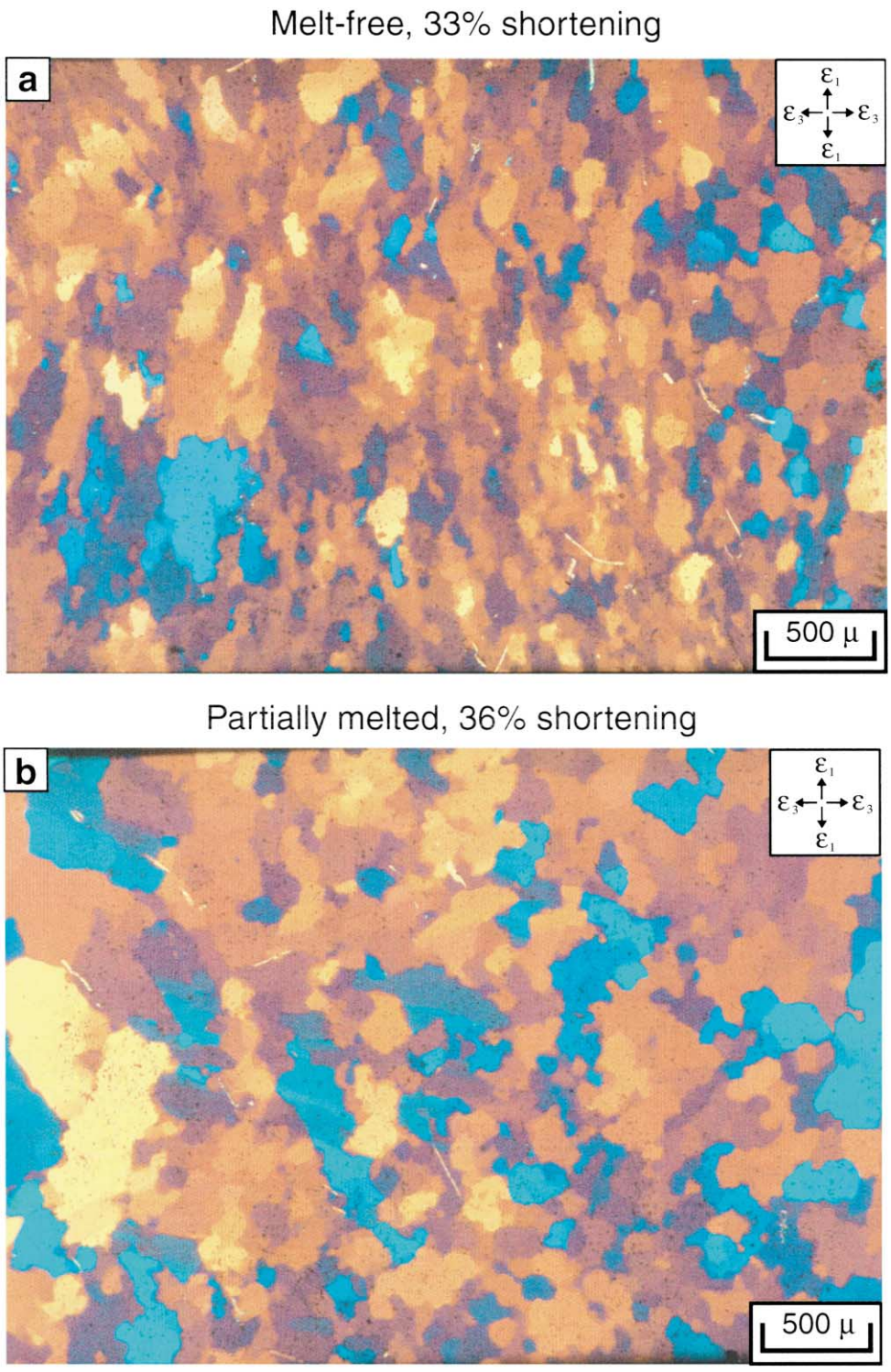

Fig. 4. Photomicrograph with crossed polarizers and a gypsum plate. (a) Norcamphor without melt shortened by 33% under pure shear conditions at 45°C. Shortening direction ($\varepsilon 3$) is horizontal. (b) Norcamphor in the presence of 10% melt of norcamphor/benzamide composition, shortened by 36% under pure shear conditions, at 45°C. Note the stronger shape- and crystallographic preferred orientations in the dry sample.

appeared and the melt content remained constant at about 12%. This precluded any increase in the sample volume during deformation and ensured that any melt migration and changes in the geometry of melt pockets and films during the experiment were due solely to shearing of the sample.

5.2. Behavior at low strains

Both before and during the first increments of strain, melt occupied pockets along grain boundaries and inclusions within norcamphor grains (Fig. 5a). The melt topology

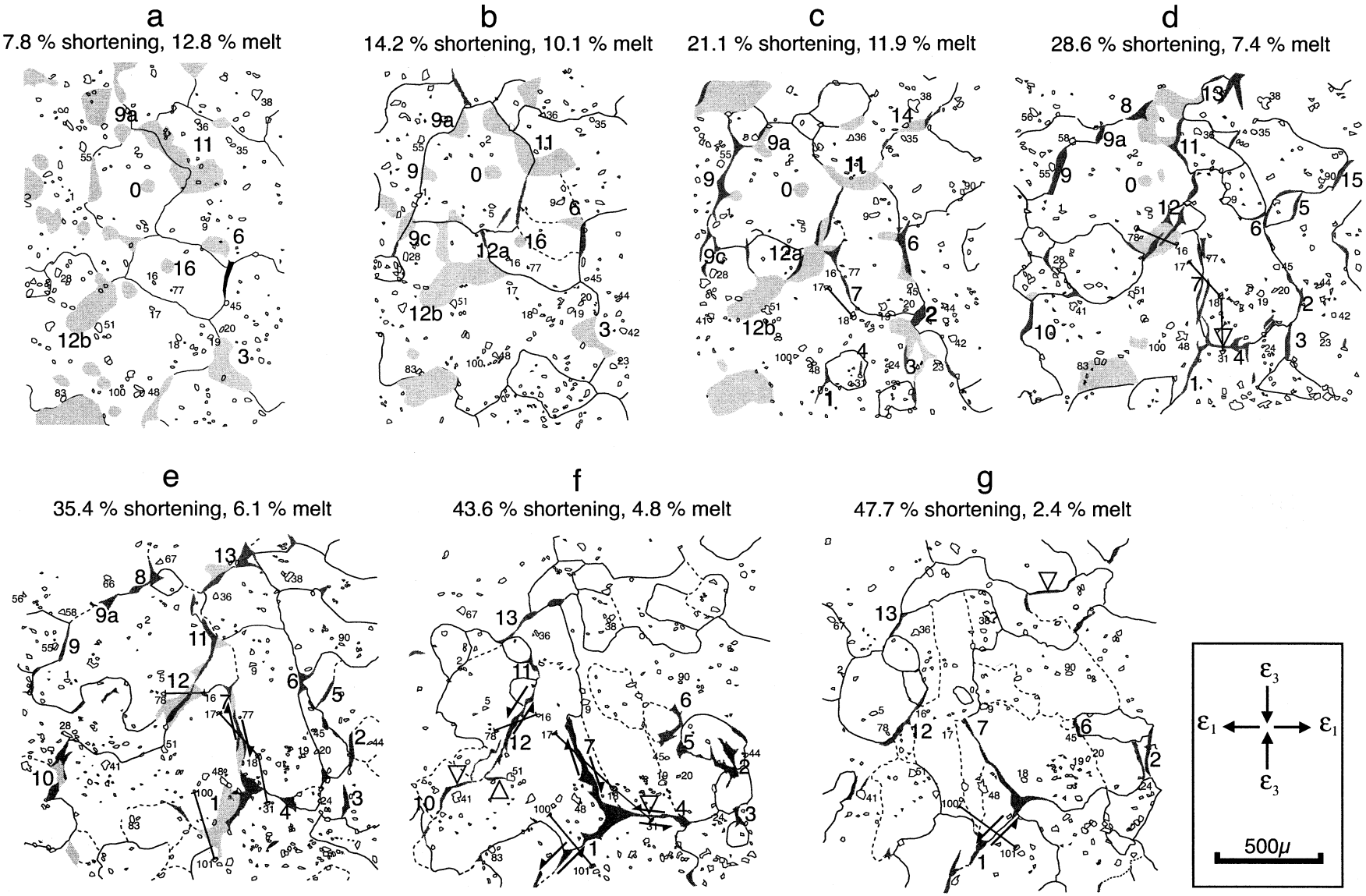

Fig. 5. Microstructural sequence (a–f) showing how the volume, shape and distribution of melt pockets change with increasing strain. Black: melt-bearing fracture; Gray: melt pockets. Stippled lines: subgrain boundaries. Small open spots: corundum markers. Large numbers refer to melt pockets, smaller numbers refer to strain markers (not all are numbered). The apparent occurrence of fractures within rounded melt pockets (as in d) is due to the truncation effect: the rounded melt pockets consist of thin melt films between the norcamphor and the upper glass plate, whereas the melt-filled fractures cross-cut the entire thickness of the sample. The percentage of melt above each frame refers to melt locally contained in the area shown. Total melt amount remained constant throughout deformation. Black bars join marker pairs to illustrate relative displacement of grains.

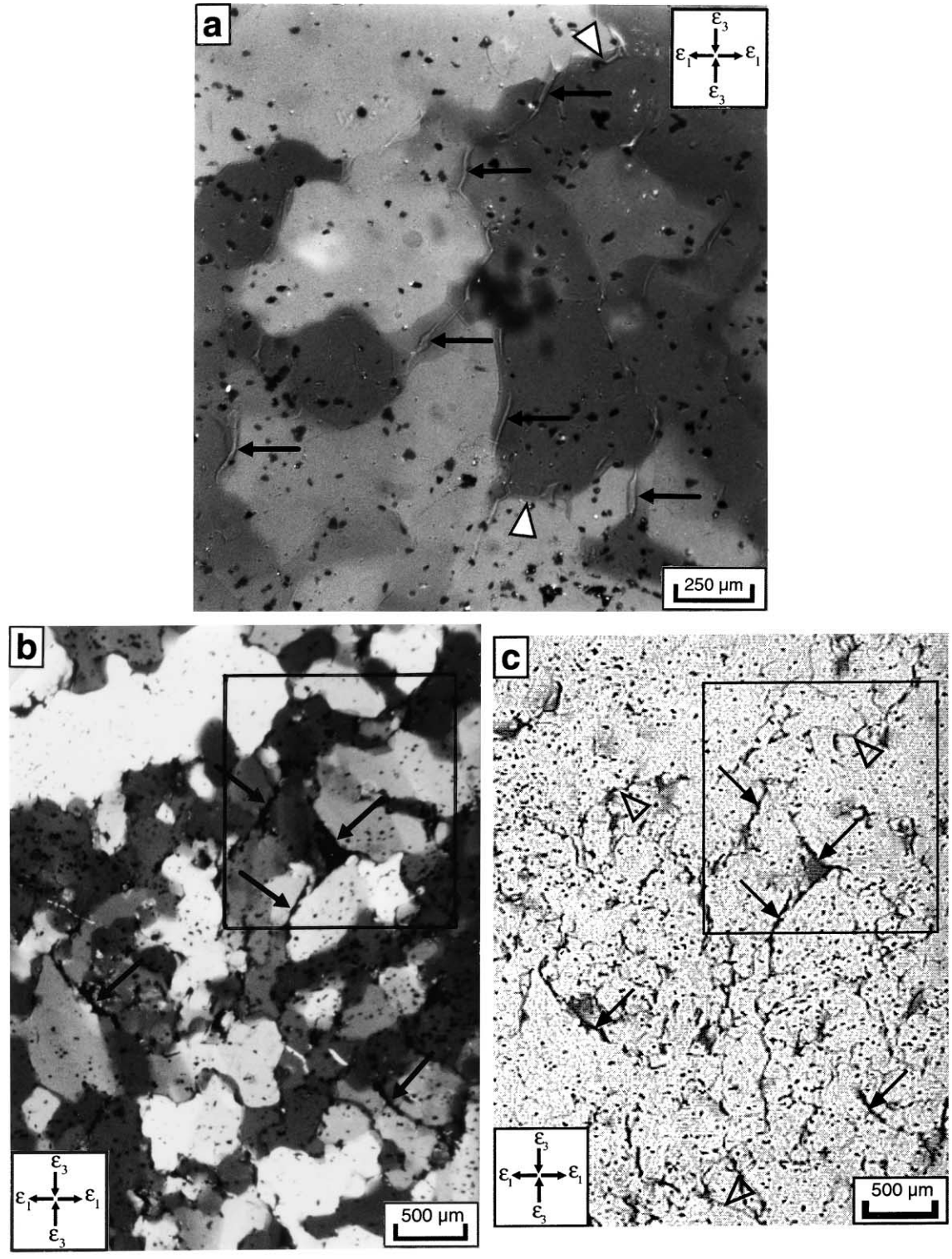

Fig. 6. (a) Micrograph of Fig. 5d, taken with reflected light in addition to crossed polarizers and gypsum plate. Melt is distributed in pockets and intergranular fractures. Arrows indicate some of the melt-bearing intergranular fractures. Open arrow heads indicate melt bearing grain boundaries subparallel to the $\varepsilon 1$ direction. Dark spots: corundum particles. (b) Micrograph of Fig. 5g with crossed polarizers, after chilling of the sample from 45 to 20°C, within approximately 1 min. Dark material along some of the grain boundaries (full arrows) is the eutectic melt that crystallized into a dark microcrystalline aggregate. Black square: area drawn in Fig. 5g. Dark spots: corundum particles. (c) Same as (b), with plane light. Open arrow heads: chilled melt along grain boundaries subparallel to extension direction $\varepsilon 1$.

was controlled solely by the pre-deformational shape and distribution of benzamide grains. Melt replaced the benzamide grains and some of the surrounding norcamphor. The resulting melt pockets had a similar shape and orientation as the pre-existing benzamide grains (see irregular orientation and shape of melt pockets in Figs. 2 and 5a).

The deformation of such a partially molten sample is shown in Fig. 5, where the microstructures within the same part of the sample are depicted at different stages of deformation. After about 15% axial shortening, melt pockets became elongate, with their long axes oriented at high angles to the principal shortening direction (Fig. 5a and b). With further deformation, melt pockets spread along grain boundaries, especially along those boundaries oriented subparallel to the principal shortening direction (Fig. 5c and d). These intergranular melt films were observed with reflected light (Fig. 6a) or by chilling of the samples, which resulted in the rapid crystallization of the melt into a dark, microcrystalline aggregate (Fig. 6b). The change in melt topology from rounded melt pockets to elongate intergranular melt films occured while the aggregate deformed by dislocation creep, as evidenced by the formation of subgrains, deformation bands, and by the deformation of individual grains (e.g. change in the relative position of markers 51 and 100 in Fig. 5a–g). Grain-boundary migration recrystallization was also active (e.g. mobile grain boundary between markers 17 and 77 in Fig. 5a–d). Grain-boundary migration recrystallization influenced the melt distribution. When intragranular melt inclusions were swept by a migrating grain boundary, they drained their melt into that grain boundary. Such was probably the fate of the melt inclusion numbered 16 in Fig. 5, which existed only during the first 14% shortening (Fig. 5a and b). With further shortening and dynamic recrystallization, this inclusion was absorbed by the migrating boundary that contained the melt pocket numbered 12a (Fig. 5c).

5.3. Moderate strain behavior

After 20% axial shortening, the melt occupied two types of site (Figs. 5c and d and 6a): (1) nearly isometric disc-shaped pockets that wedged out against neighbouring grains (light gray in Fig. 5); and (2) intergranular elongate lenses or films (marked with arrows in Fig. 6a, and black in Fig. 5). The isometric pockets formed during static melting. They replaced the benzamide grains and parts of the norcamphor grains originally surrounding the benzamide. Such pockets had nearly isometric shapes in the $\varepsilon 1$–$\varepsilon 3$ plane before deformation started and became slightly elongate parallel to the maximum extensional direction during deformation. The elongate intergranular melt lenses had high aspect ratios and, with few exceptions, they were oriented subparallel to the principal shortening direction (Figs. 5c and d and 6). We use the term rounded melt pockets for sites containing melt that formed during coeval stress-annealing and melting of the sample. The term intergranular melt pockets will be used to refer to sites of melt accumulation that formed after the onset of deformation along grain boundaries. The geometry and orientation of the intergranular melt pockets subparallel to the $\varepsilon 3$ direction suggest intergranular extensional fracturing, but the width of these melt pockets was only 2% of the grain diameter (approximately 10 μm), and thus precluded an unequivocal identification of dilation even at maximum magnification (64×). Several authors have argued against fracturing for the formation of similarly oriented melt pockets during experimental deformation of partially molten mantle rocks (Bussod and Christie, 1991; Daines and Kohlstedt, 1997; Zimmerman et al., 1999). Nevertheless, the following observations support microcracking as the grain-boundary dilation mechanism in our experiments: (1) the tips of the melt pockets was sharp (Fig. 6a), as expected for propagating fractures; and (2) the transition from isotropic to elongate intergranular melt pockets occured abruptly and there was no evidence for gradual growth of these melt pockets along the grain boundaries. In fact, they formed so rapidly that they could not be resolved by our time slices (one picture every 6 min, i.e. after shortening increments of approximately 0.3%).

An alternative explanation that the grain boundary films merely represent wetting of grain boundaries (presuming a wetting angle $<60°$) is inconsistent with the strong preferred orientation of these films related to the kinematic framework in our samples.

Figs. 5d and f and 6a also show that, locally, melt can be found along grain boundaries oriented parallel to the $\varepsilon 1$ direction (see open arrows). However, the presence of melt along grain boundaries with this orientation was short-lived. As shown by Fig. 5e and g, the aforementioned grain boundaries were dry again after a small strain increment.

At yet higher coaxial strains (about 35%), the intergranular melt pockets became more abundant and the rounded melt pockets disappeared (Fig. 5e). The rounded pockets appear to drain their melt into the fractures. This can be seen in the deformational sequence in Fig. 5: a melt-filled fracture develops near the melt pocket numbered 6 (Fig. 5b and c) and gradually draws all the melt from the pocket into the open grain boundary (Fig. 5c and d). Dislocation creep and dynamic recrystallization are still active during this stage of fracturing, as shown by the migrating grain boundaries, the occurrence of subgrains and deformation bands, and the relative displacements of the strain markers within individual grains (Fig. 5).

5.4. High strain behavior

At an axial shortening of about 40%, intergranular melt pockets tended to coalesce (Fig. 5f). Upon coalescing, the preferred orientation of the fractures subparallel to the principal shortening direction decreased (Fig. 5f). The fractures appear to rotate slightly during deformation. At yet higher

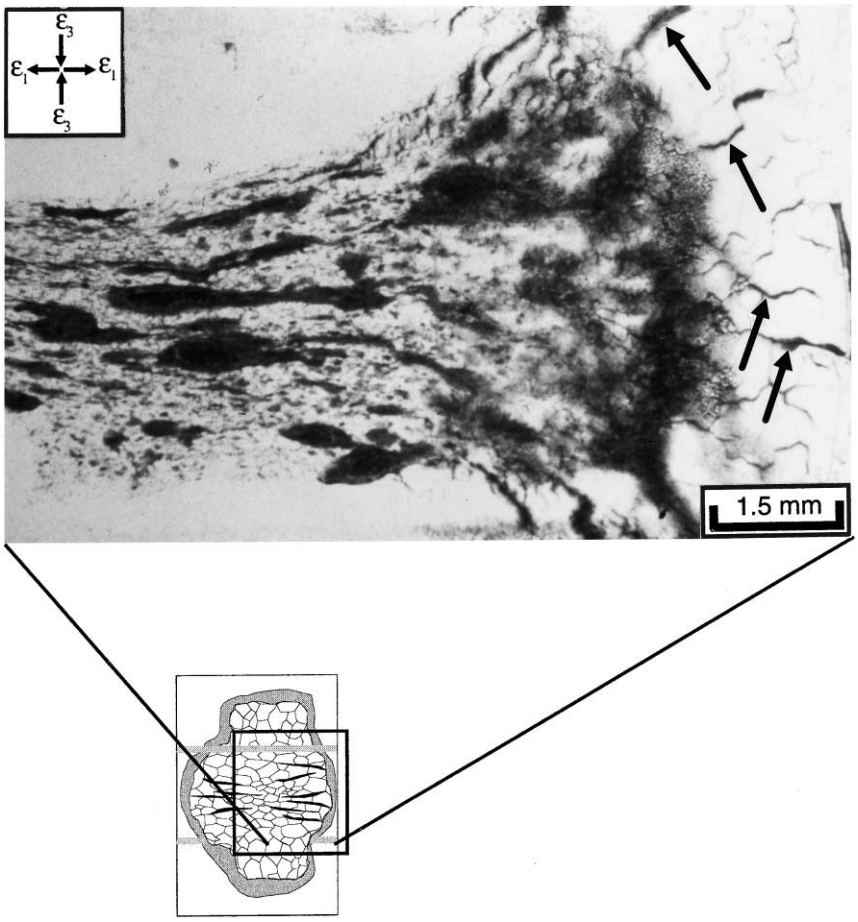

Fig. 7. Sample consisting of 10% benzamide, and 90% norcamphor, deformed in the partially molten state, and chilled at the end of deformation. The benzamide content is higher than that used for the experiment illustrated in Figs. 5 and 6, but all other experimental conditions are identical. Dark areas in the central part of the sample are benzamide aggregates that did not melt by the end of the experiment. These aggregates mark the foliation plane (F). Dark patches and films at the side of the picture (black arrows) represent melt chilled to a microcrystalline aggregate. Melt was extruded 'sideways', into extensional fractures that formed in the 'barrelled' part of the sample. Horizontal black lines are the margins of the frosted grips.

coaxial strains, most melt left the middle of the sample (Fig. 5g) and migrated to the sample's edges, outside the field of view in Fig. 5. This indicates that melt segregation occurred at melt fractions lower than 5% (see discussion below). An interesting feature that was not observed at lower strain was the onset of grain boundary sliding (GBS) along those boundaries that were coated with melt. GBS can be identified by comparing the relative position of strain markers in individual grains with the position of markers between grains during a deformational sequence. For example, the sequence in Fig. 5d–g shows that dextral shearing occurred along the grain boundary between the strain markers numbered 48 and 18, whereas the relative position of the strain markers numbered 18 and 45 within a single grain remained constant throughout the deformational sequence. The onset of GBS appears to coincide with the coalescence of melt-filled fractures.

Despite the general orientation of the melt-bearing fractures throughout the deformation sequence (Fig. 5), melt segregation occurred in a direction perpendicular to these fractures. This is shown in Fig. 5, where melt extruded from the sample in a direction parallel to that of the foliation plane, i.e. parallel to the flattening plane. Melt accumulated at both sides of the sample, where barrelling occurred (see inset of Fig. 7) and fractures formed perpendicular to the imposed shortening direction (Fig. 7). Dell'Angelo and Tullis (1988) referred to this process as lateral flow. The deformation sequence illustrated in Fig. 5 shows that even in the middle of the sample, melt can spread along grain boundaries perpendicular to the shortening direction (arrows in Figs. 5d and f and 6a). Melt films disappeared very rapidly from such sites, however, and could not be observed in the subsequent deformational increment (photographs were taken at intervals of 2% shortening). The sample quenched after deformation shows that melt films perpendicular to the shortening direction were rare (open arrows in Fig. 6c) and that their width was thinner than the melt films subparallel to the shortening direction. Unfortunately, we were unable to determine whether melt spreading along grain boundaries oriented perpendicular to $\varepsilon 3$ also occurred by intergranular fracturing. However, the spreading of melt along these grain boundaries indicates that: (1)

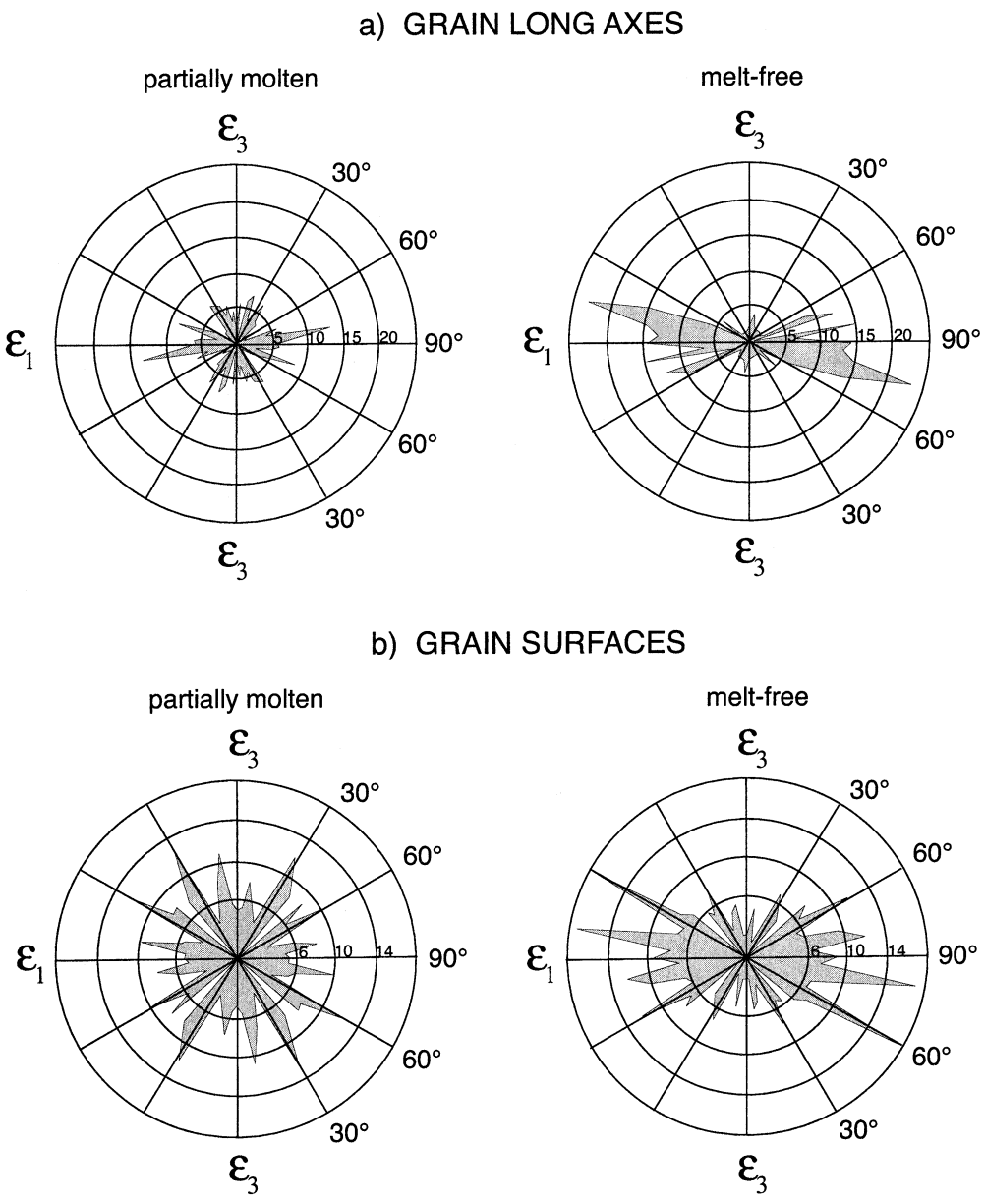

Fig. 8. Rose diagrams. showing orientation of long axes of grains (PAROR) (a) and orientation of grain surfaces (SURFOR) (b). Rose diagrams on the left for a sample shortened 38.5% in the presence of melt. Diagrams on the right for a sample shortened 40% under dry conditions.

melt can migrate along grain boundaries in a direction perpendicular to the shortening direction, and (2) expulsion of melt from such sites is more rapid than along grain boundaries oriented subparallel to the shortening direction. Although the presence of melt along grain boundaries parallel to the $\varepsilon 1$ direction was ephemeral, melt flux along these boundaries appears to have been high enough to allow melt segregation parallel to the $\varepsilon 1$ direction. As melt could not flow through the frosted grips, it could only exit through the sides of the sample. With these experimental boundary conditions we have established that, despite the numerous intergranular fractures perpendicular to $\varepsilon 1$, flow occurred in the $\varepsilon 1$ direction provided that a melt pressure gradient existed in that direction.

5.5. Comparison with melt-free experiments

As shown in Fig. 4, the shape and orientation of norcamphor grains varied markedly as a function of melt-presence. In order to quantify the effect of melt on the shape and orientation of the solid grains, micrographs from the samples above, deformed in both the presence and absence of melt, were analyzed using image analysis techniques. The programs PAROR and SURFOR (Panozzo, 1983, 1984) were used to characterize the particle and surface orientation of grains, respectively. The results of the image analysis are shown in Fig. 8 for a sample shortened 38.5% in the presence of melt and a sample shortened 40% under dry conditions. Fig. 8a shows that the preferred orientation of

the long axes of norcamphor grains deformed in the absence of melt was very strong and subperpendicular to the imposed shortening direction ($\varepsilon 3$) of the sample. In contrast, in the presence of melt (Fig. 8a) both the preferred orientation and the axial ratios of norcamphor grains were weaker. The difference in surface orientation of grains in dry and melt-added experiments was even more dramatic (Fig. 8b). Samples deformed in the presence of melt showed that grain boundaries did not have any significant preferred orientation, whereas dry samples showed a strong preferred orientation of grain boundaries subperpendicular to the imposed shortening direction. These observations, in addition to the constant orientation of melt films subparallel to the shortening direction during deformation (Fig. 5), suggest that grain boundaries filled by melt did not change their orientation during deformation, i.e. they are locked by the melt. The lower axial ratios of the grains in the presence of melt may reflect the melt-enhanced activity of GBS in addition to dislocation creep.

6. Discussion

6.1. How does melt induce changes in the deformation mechanisms of the norcamphor grains?

Melt enhances both intergranular fracturing and GBS. As shown by the deformation sequence in Fig. 5, GBS is restricted to grain boundaries wetted by melt. Fractures are always filled with melt and are located at grain boundaries that were previously occupied by melt pockets (Fig. 5). Where there was no melt, there are no fractures. Moreover, no fractures were observed in the melt-free experiments. Melt is therefore the agent controlling fracturing. This can be explained by the ability of melt to exert a pore-fluid pressure (Shaw, 1980) opposite to the normal stress on grain boundaries during deformation, and thus to reduce the effective stress. Intergranular fractures rather than intragranular fractures are expected to form in partially-molten systems, because failure at high homologous temperatures and low stresses is always by intergranular creep fracture (Gandhi and Ashby, 1979).

Fracturing is especially important during the transition from a structure in which melt occupies rounded pockets to one in which melt is distributed along grain boundaries (Fig. 5c and d). Once the melt is distributed primarily along grain boundaries (Fig. 5e and f), fracturing becomes less important and the increased spreading of melt along grain boundaries facilitates GBS despite the very large grain size (approximately 500 μm).

6.2. How does melt topology relate to grain scale deformation mechanisms?

Bussod and Christie (1991) and Jin et al. (1994) showed that deformation enhances the distribution of melt along olivine grain boundaries. Jin et al. (1994) and Bai et al. (1997) referred to this process as dynamic wetting of grain boundaries, but stated that the mechanisms driving this process are not yet understood. Kohlstedt and Zimmerman (1996), Daines and Kohlstedt (1997), Gleason et al. (1999) and Zimmerman et al. (1999) also observed that deformation induces melt spreading along grain boundaries provided that differential stresses are high (higher than 100–160 MPa in their experiments). Moreover, as already described by Bussod and Christie (1991), they noted a preferred orientation of the long axes of melt pockets at an angle of 15–20° to the principal compressive stress direction. Daines and Kohlstedt (1997) and Zimmerman et al. (1999) suggested that this preferred orientation of melt pockets is induced by sample-scale gradients in mean pressure rather than by fracturing. They argue this because the long axes of the melt pockets are not oriented parallel to the principal stress direction and because microfracturing is not observed in their samples (previously argued by Bussod and Christie (1991)); also, the stress exponent was too low ($n = 1$) for a material undergoing microfracturing. However, the stress exponent is probably not a diagnostic criterion for precluding fracturing if fracturing is not the dominant deformation mechanism. This is the case in our experiments, where intergranular fracturing was clearly subordinate to dislocation creep and GBS, such that the influence of fracturing on the value of the stress exponent was probably small.

By analogy with the experiments of Bussod and Christie (1991), Kohlstedt and Zimmerman (1996) and the high-stress experiments of Daines and Kohlstedt (1997) and Gleason et al. (1999), the microstructures in our experiments also indicate stress-induced spreading of melt along grain boundaries associated with the development of a preferred orientation of melt pockets subparallel to the incremental shortening direction (see Fig. 5). The microstructural evolution during deformation of our analog materials suggests that dynamic wetting of grain boundaries results from intergranular fracturing and that it is later masked by GBS and/or dissolution that transform the originally planar, fracture surfaces (Fig. 5d) into more irregular non-planar ones (Fig. 5f). This overprinting effect may also operate in mantle rocks and hence mask the fracture-related origin of many intergranular pockets. Intergranular fracturing may explain the controversial process underlying dynamic wetting of grain boundaries (Jin et al., 1994), i.e. the process by which entire grain boundaries are wetted by melt during deformation, even though the equilibrium dihedral angles between grains and melt are $\geqslant 0$.

In contrast to intragranular fractures, intergranular fractures may be difficult to identify in nature and experiment for the following reasons: (1) no offset or dissection of markers (e.g. twinning planes or deformation bands) can be observed; (2) the shape of these fractures is controlled by the pre-existing shape of grain boundaries, which may be lobate and non-planar, in contrast to the more commonly

observed planar geometry of fractures; and (3) the original shape and orientation of melt-bearing fractures may be modified by subsequent sliding of grains along the melt-bearing boundaries. As a consequence, the identification of these melt pockets as intergranular fractures also depends on the amount of deformation suffered by the rock after intergranular fracturing.

6.3. Does the presence of melt enhance grain boundary migration recrystallization?

The experiments of Bai et al. (1997) on peridotites showed that melt enhances grain-boundary migration rates in olivine, whereas Hirth and Kohlstedt (1995) found that grain-boundary migration is inhibited in olivine aggregates that were deformed in the presence of basaltic melt. Dell'Angelo and Tullis (1988) also observed increased grain-boundary migration recrystallization during syntectonic melting of aplite, but attributed this to the presence of water rather than melt.

Our pure shear experiments show that melt induced very rapid grain boundary migration and grain growth under stress-annealing conditions, but the effect of melt on synkinematic grain-boundary migration is more complex. The highly lobate geometry of grain boundaries in the partially-molten sample (Fig. 4b) indicates that grain-boundary migration recrystallization was an important process during deformation in the presence of melt. However, within the partially-molten sample the melt-bearing grain boundaries were more stable than the melt-free grain boundaries throughout the deformational sequence. In Fig. 5, for example, the melt-bearing grain boundary separating markers 77 and 18 from markers 16 and 17 was stable from 21 to 43% axial shortening. In contrast, melt-free grain boundaries migrated much more rapidly during a similar strain increment (Fig. 5). Moreover, comparison of Fig. 6b and c shows that lobate grain boundaries were melt-free, whereas melt-bearing grain boundaries tended to be straight. Melt-bearing grain aggregates show a less pronounced SPO and a larger proportion of grain boundaries oriented subparallel to the principal shortening direction (Figs. 5 and 8). In comparison, melt-free norcamphor aggregates deformed at the same axial strain rate and temperature developed a strong SPO defined by the long axes of dynamically recrystallized grains oriented subparallel to the principal extensional direction (Figs. 4 and 8). Hirth and Kohlstedt (1995) observed similar microstructural differences in melt-bearing and melt-free olivine aggregates in their high pressure experiments. The weaker SPO of the partially molten aggregates reflects the stability of melt-bearing grain boundaries oriented parallel to the principal shortening direction. Thus, melt inhibits grain-boundary migration during dynamic recrystallization at the experimental conditions in this study. Urai et al. (1986) suggested that fluids enhance the rate of grain boundary migration recrystallization and that increasing thickness of the fluid films enhances the rate of migration up to a critical thickness of approximately 20 nm. Any further increase of fluid thickness reduces the rate of migration. The thickness of intergranular melt films in our samples (Figs. 5 and 6) is higher than 20 nm by several orders of magnitude (5–50 μm). This is consistent with the model of Urai et al. (1986), which predicts that grain boundary migration is inhibited by thick melt films. Note that melt films of a similar width to those observed in our experiments are inferred to occur in natural, dynamically recrystallized quartz aggregates in the presence of granitic melt (Rosenberg and Riller, 2000).

6.4. What effect does deformation have on the percolation threshhold and segregation?

Our experiments indicate that melt can migrate through a deforming crystalline aggregate at much lower volume proportions than previously thought. It is commonly believed that melt segregation can only occur once the melt forms an interconnected network throughout the melting protolith (e.g. Maaløe, 1985; Sawyer, 1994; Vigneresse et al., 1996). Several authors have estimated the minimum melt fraction at the onset of melt segregation; values ranging from less than 5% (Sawyer, 1994) to 8% (Vigneresse et al., 1996) have been proposed. Recent experimental work under static conditions (Laporte et al., 1997) showed, however, that melt channels in granite may be very thin (<0.3 μm), thus allowing interconnection at melt volumes as small as 0.04%. Under these conditions it is suggested that the viscosity of the melt, rather than its volume fraction controls the ability of melt to escape from its source region (Laporte et al., 1997).

Our experiments show that, under dynamic conditions, melt migration in norcamphor occurred at melt fractions as low as 0.01–0.05. This is illustrated in Fig. 5, where the gradual reduction in melt fraction from 0.048 to 0.01 during the stages shown in Fig. 5e and f indicates that melt exited the investigated area of the sample. Melt pockets were not connected at low strains (Fig. 5a), but intergranular fracturing during deformation eventually lead to the interconnection (Fig. 5c). During the final stages of defor-mation more melt drained from the melt-source area, hence reducing the melt fraction and also interconnection. Interconnection parallel to the shortening direction was maintained up to the end of deformation (Fig. 6c), but interestingly did not occur in the main flow direction, i.e. from the center to the extending ends of the sample (Fig. 7), at least not on the scale of observation of our experimental set-up (maximum magnification 64×). Nevertheless, the melt content in Fig. 5g was smaller than that in Fig. 5f, suggesting that the melt was still segregating. Note that we can exclude the escape of melt along the interface between glass and sample (*XY* plane) because quenching of the samples at the end of deformation always revealed chilled melt (Fig. 6b and c) along the grain boundaries (at high angles to the *XY* plane) and never parallel to the

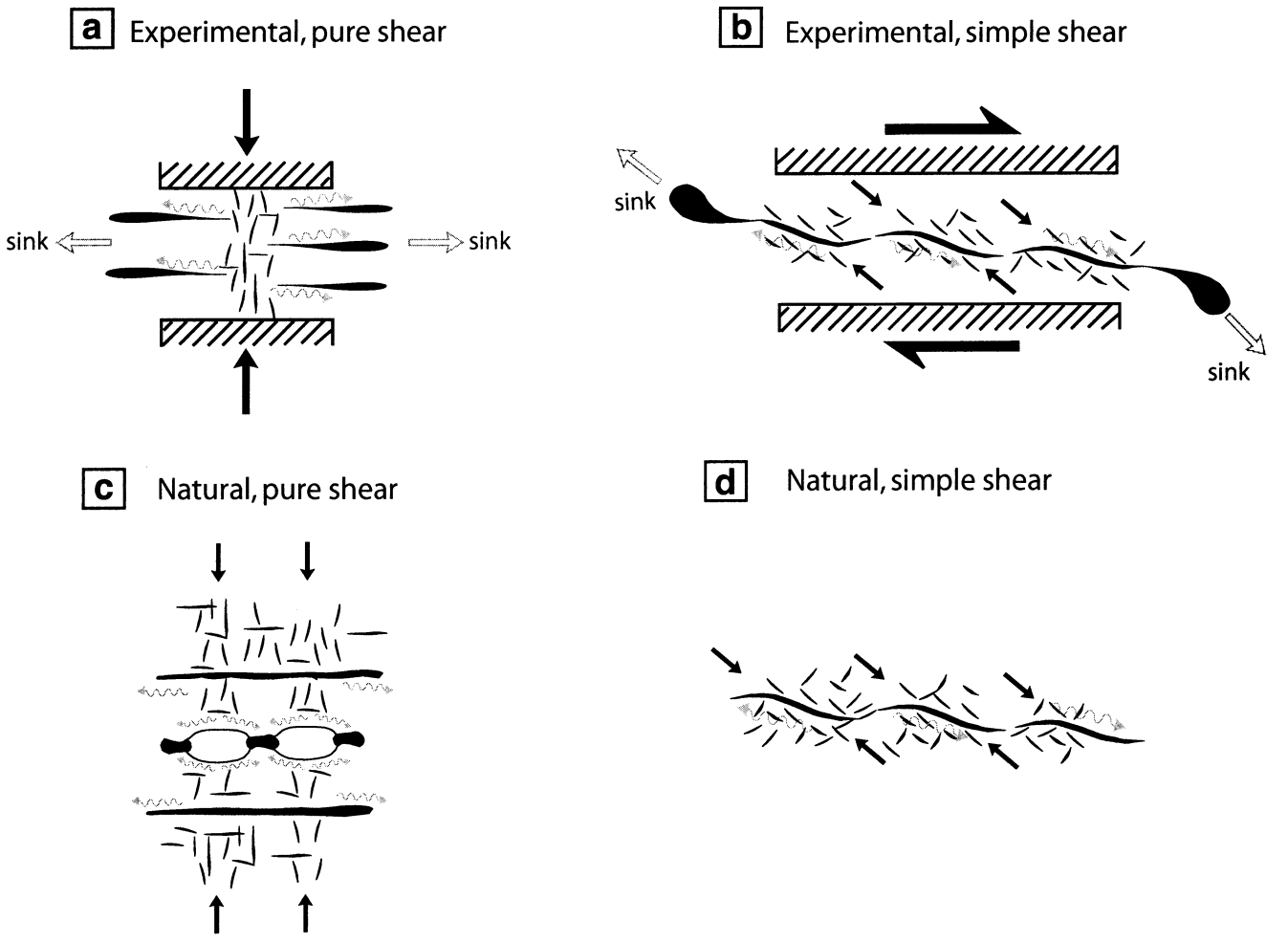

Fig. 9. Schematic drawings illustrating the relationship between shortening direction, location of melt sinks, and segregation direction of melt in a deforming partially molten aggregate. Black: melt pockets. Full arrows: incremental shortening direction. Gray arrows: melt flow direction.

glass plate (*XZ* plane). This suggests that melt segregation at melt fractions lower than 0.05 (Fig. 5f and g) occurred along transient, short-lived melt-channels rather than through a stable network of interconnected melt pathways.

6.5. Preservation of synmagmatic microstructures

Except for the melt films and pockets observed along the grain boundaries, microstructures of norcamphor deformed in the presence of 2–12% melt look similar to commonly observed microstructures of quartz deformed under high-temperature, solid-state conditions (lobate grain boundaries, deformation bands, subgrains of irregular shape). However, the shape and orientation of dynamically recrystallized grains in the presence of melt are different: the SPO is only weak or absent, whereas it is very strong in the absence of melt (Fig. 8). This difference in the strength of the SPO between melt-bearing and melt-free aggregates was also observed by Hirth and Kohlstedt (1995) in experimentally deformed, partially molten olivine samples at high pressure (300 MPa). This difference in the SPO may serve as a diagnostic criterium to identify microstructures resulting from synmagmatic deformation.

7. Conclusions and geological implications

Our experiments show that melt, even in small amounts, modifies the deformation of a polycrystalline aggregate in several ways. It induces intergranular fracturing in an aggregate that, in the absence of melt at the same temperature and strain rate, deforms by dislocation creep. These fractures enhance the distribution of melt along grain boundaries, thereby inhibiting grain-boundary migration and favouring GBS. The onset of GBS in the presence of melt in the dislocation creep regime is known to reduce the strength of partially molten olivine aggregates (Jin et al., 1994; Hirth and Kohlstedt, 1995). Although we were unable to measure the strength of our samples, by analogy with these experimental investigations, we can infer that weakening induced by GBS is more pronounced than

hardening due to the inhibition of grain-boundary migration recrystallization.

Several processes widely inferred to occur in experimentally deformed, partially molten rocks were also observed in our 'see-through' experiments: (1) dynamic wetting of grain boundaries (Jin et al., 1994); (2) melt-induced fracturing during dynamic recrystallization (Dell'Angelo and Tullis, 1988); (3) melt-inhibited grain boundary migration (Hirth and Kohlstedt, 1995); and (4) melt-enhanced GBS (e.g. Jin et al., 1994). These processes were also believed to occur in nature. Melt-induced fracturing during dynamic recrystallization and dynamic wetting of grain boundaries were inferred to operate in partially molten orthogneisses (Rosenberg and Riller, 2000); melt-enhanced GBS was inferred to control deformation of partially molten gabbros (Nicolas and Ildefonse, 1996). Our experiments show that the latter mechanism is very difficult to identify in the absence of strain markers, especially if this mechanism operated during dynamic recrystallization. This suggests that melt-enhanced GBS may be much more common than previously thought.

Fig. 9 summarizes the relationships between melt pathways and the kinematics of deformation in this and previous experiments, as well as in nature. It shows that melt pathways are determined primarily by melt pressure gradients between melt source areas and melt sinks, rather than by the kinematics of deformation. For example, the melt flow direction in pure shear experiments is from the center to the sides of the sample, subparallel to the shearing plane and extensional direction, whereas in simple shear, melt migrates oblique to the shearing plane and subparallel to the main shortening direction (compare Fig. 9a and b). Similar melt flow directions with respect to the kinematic regime can be inferred in nature for the near end-member pure and simple shear configurations (Fig. 9c and d). Not all melt pathways are equally well preserved, however. The extent to which melt pathways are visible or even preserved strongly depends on whether the melt pressure gradients were subparallel or subperpendicular to the principal strain axes. In the case of simple-shear dominated deformation, the melt pressure gradient is subparallel to dilatant shear bands, which open subparallel to the principal shortening direction and remain open to high shear strains as they maintain strain compatibility in the aggregate. In pure shear deformation, however, the lateral melt pressure gradient induces the opening of intergranular channels perpendicular to the shortening direction; these channels are necessarily short-lived because they tend to be closed during deformation to maintain compatibility.

To conclude, deformation-induced melt pathways do not necessarily coincide with the main pathways determined by melt pressure gradients. This suggests that large-scale melt migration, for example beneath mid-ocean ridges (e.g. Daines and Kohlstedt, 1997), may be subparallel rather than highly oblique to the structural anisotropies induced by anatectic or solid-state creep in the host rock.

7. Uncited References

Brown, 1994. Brown et al., 1999. Dell'Angelo et al., 1987. Jessel, 1986. Rutter, 1997.

Acknowledgements

We acknowledge financial support of the German Science Foundation in the form of DFG-project Ha-2403/2 (SPP "Orogene Prozesse…") and Ro-2177-1 ("Bildung, Transport und Differenzierung von Silikatschmelzen"). P. Bauer is thanked for helpful discussions. T. Rushmer, J.L. Vigneresse, an anonymous reviewer and Jim Evans made many useful suggestions.

References

Bai, Q., Jin, Z.-M., Green II, W., 1997. Experimental investigation of the rheology of partially molten peridotite at upper mantle pressures and temperatures. In: Holness, M.B. (Ed.). Deformation-enhanced Fluid Transport in the Earth's Crust and Mantle. Chapman & Hall, pp. 40–61 The Mineralogical Society Series 8.

Bauer, P., Rosenberg, C., Handy, M.R., 2000. 'See-through' deformation experiments on brittle-viscous norcamphor at controlled temperature, strain rate and applied confining pressure. Journal of Structural Geology 22, 281–289.

Berger, A., Kalt, A., 1999. Structures and melt fractions as indicators of rheology in cordierite-bearing migmatites of the Bayerische Wald (Variscan Belt, Germany). Journal of Petrology 40, 1699–1719.

Bodinier, J.L., 1988. Geochemistry and petrogenesis of the Lanzo peridotite body, western Alps. Tectonophysics 149, 67–88.

Bons, P., 1993. Experimental deformation of polyphase rock analogs. Geol. Ultrajectina 110, 207.

Brown, M., 1994. The generation, segregation, ascent and emplacement of granite magma: the migmatite-to-crustally-derived granite connection in thickened orogens. Earth Science Reviews 36, 83–130.

Brown, M.A., Brown, M., Carlson, W.D., Denison, C., 1999. Topology of syntectonic melt flow networks in the deep crust: inferences from three-dimensional images of leucosome geometry in migmatites. American Mineralogist 84 (11-12), 1793–1818.

Bussod, G.Y., Christie, J.M., 1991. Textural development and melt topology in spinel lherzolite experimentally deformed at hypersolidus conditions. Journal of Petrology, Special lherzolite issue, 17–39.

Daines, M.J., 1997. Melt distribution in partially molten peridotites: implications for permeability and melt migration in the upper mantle. In: Holness, M.B. (Ed.). Deformation-enhanced Fluid Transport in the Earth's Crust and Mantle. Chapman & Hall, pp. 62–81 The Mineralogical Society Series 8.

Daines, M.J., Kohlstedt, D.L., 1997. Influence of deformation on melt topology in peridotites. Journal of Geophysical Research 102, 10257–10271.

Dell'Angelo, L.N., Tullis, J., 1988. Experimental deformation of partially melted granitic aggregates. Journal of Metamorphic Geology 6, 495–515.

Dell'Angelo, L.N., Tullis, J., Yund, R.A., 1987. Transition from dislocation creep to melt-enhanced diffusion creep in fine-grained granitic aggregates. Tectonophysics 139, 325–332.

Gandhi, C., Ashby, M.F., 1979. Fracture-mechanism maps for materials which cleave: F.C.C., B.C.C. and H.C.P. metals and ceramics. Acta Metallurgica 27, 1565–1602.

Gleason, G.C., Bruce, V., Green, H.W., 1999. Experimental investigation of melt topology in partially melted quartzo–feldspathic aggregates

under hydrostatic and non-hydrostatic stress. Journal of Metamorphic Geology 17, 705–722.

Herwegh, M., Handy, M.R., 1996. The evolution of high-temperature mylonitic microfabrics: evidence from simple shearing of a quartz analog (norcamphor). Journal of Structural Geology 18, 689–710.

Hirth, G., Kohlstedt, D.L., 1995. Experimental constraints on the dynamics of the partially molten upper mantle. 2. Deformation in the dislocation creep regime. Journal of Geophysical Research 100, 15441–15449.

Jessel, M.W., 1986. Grain boundary migration and fabric development in experimentally deformed octachloropropane. Journal of Structural Geology 8, 527–542.

Jin, Z., Green, H.W., Zhou, Y., 1994. Melt topology in partially molten mantle peridotite during ductile deformation. Nature 372, 164–167.

Jousselin, D., Mainprice, D., 1999. Melt topology and seismic anisotropy in mantle peridotites of the Oman ophiolite. Earth and Planetary Science Letters 164, 553–568.

Kohlstedt, D.L., Zimmerman, M.E., 1996. Rheology of partially molten mantle rocks. Annual Reviews of Earth and Planetary Science 24, 41–62.

Laporte, D., Rapaille, C., Provost, A., 1997. Wetting angles, equilibrium melt geometry, and the permeability threshold of partially molten crustal protholiths. In: Bouchez, J.L., Hutton, D.H.W., Stephens, W.E. (Eds.). Granite: From Segregation of Melt to Emplacement Fabrics. Kluwer Academic, Dordrecht, pp. 31–54.

Maaløe, S., 1985. Principles of Igneous Petrology. Springer Verlag, Berlin 374 p.

McLellan, E., 1988. Migmatite structures in the Central Gneiss Complex, Boca de Quadra, Alaska. Journal of Metamorphic Geology 6, 517–542.

Means, W.D., 1983. Microstructure and micromotion in recrystallization flow of octachloropropane: a first look. Geologische Rundschau 72, 511–528.

Means, W.D., 1989. Synkinematic microscopy of transparent polycrystals. Journal of Structural Geology 11, 163–174.

Mehnert, K.R., Büsch, W., Schneider, G., 1973. Initial melting at grain boundaries of quartz and feldspar in gneisses and granulites. Neues Jahrbuch der Mineralogie Monatshefte, 165–183.

Nicolas, A., Jackson, M., 1982. High temperature dikes in peridotites: origin by hydraulic fracturing. Journal of Petrology 23, 568–582.

Nicolas, A., Ildefonse, B., 1996. Flow mechanism and viscosity in basaltic magma chambers. Geophysical Research Letters 23, 2013–2016.

Panozzo, R., 1983. Two-dimensional analysis of shape fabric using projections of digitized lines in a plane. Tectonophysics 95, 279–294.

Panozzo, R., 1984. Two-dimensional strain from the orientation of lines in a plane. Journal of Structural Geology 6, 215–221.

Rasband, W., 1997. Image 1.61. Public Domain Software. National Institute of Health. Research Services Branch NIMH, Bethesda, Maryland.

Rosenberg, C.L., Handy, M.R., 2000. Syntectonic melt pathways during simple shearing of an anatectic rock analog (norcamphor–benzamide). Journal of Geophysical Research 105, 3135–3149.

Rosenberg, C.L., Riller, U., 2000. Differences in partial melt topology in statically and dynamically crystallized granitoids. Geology 28, 7–10.

Rubin, A.M., 1997. Dike ascent in partially melted rock. Journal of Geophysical Research 103, 20901–20919.

Rutter, E.H., 1997. The influence of deformation on the extraction of crustal melts: a consideration of the role of melt-assisted granular flow. In: Holness, M.B. (Ed.). Deformation-enhanced Fluid Transport in the Earth's Crust and Mantle. Chapman & Hall, pp. 82–110 The Mineralogical Society Series 8.

Sawyer, E., 1994. Melt segregation in the continental crust. Geology 22, 1019–1022.

Shaw, H.R., 1980. Fracture mechanisms of magma transport from the mantle to the surface. In: Hargraves, R.B. (Ed.). Physics of Magmatic Processes. Princeton University Press, Princeton, pp. 201–264.

Urai, J.L., Means, W.D., Lister, G.S., 1986. Dynamic recrystallization of minerals. In: Hobbs, B.E., Heard, H.C. (Eds.). Mineral and Rock Deformation: Laboratory Studies—The Paterson Volume, pp. 161–199 American Geophysical Union Geophysical Monographs 36.

Vigneresse, J.L., Barbey, P., Cuney, M., 1996. Rheological transitions during partial melting and crystallization with application to felsic magma segregation and transfer. Journal of Petrology 37, 1579–1600.

Weber, C., Barbey, P., 1986. The role of water, mixing processes and metamorphic fabric in the genesis of the Baume migmatites (Ardèche, France). Contributions to Mineralogy and Petrology 92, 481–491.

Weijermars, R., 1986. Flow behaviour and physical chemistry of bouncing putties and related polymers in view of tectonic laboratory applications. Tectonophysics 124, 325–358.

Zimmerman, M.E., Zhang, S., Kohlstedt, D.L., Karato, S., 1999. Melt distribution in mantle rocks deformed in shear. Geophysical Research Letters 26, 1505–1508.